Author/s:
Han, Y;Zhou, J;Hu, Y;Lin, Z;Ma, Y;Richardson, JJ;Caruso, F

Title:
Polyphenol-based nanoparticles for intracellular protein delivery via competing supramolecular interactions

Date:
2020-10-27

Citation:
Han, Y., Zhou, J., Hu, Y., Lin, Z., Ma, Y., Richardson, J. J. & Caruso, F. (2020). Polyphenol-based nanoparticles for intracellular protein delivery via competing supramolecular interactions. ACS Nano, 14 (10), pp.12972-12981. https://doi.org/10.1021/acsnano.0c04197.

Persistent Link:
https://hdl.handle.net/11343/245494

Polyphenol-Based Nanoparticles for Intracellular Protein Delivery *via* Competing Supramolecular Interactions

*Yiyuan Han, Jiajing Zhou, Yingjie Hu, Zhixing Lin, Yutian Ma, Joseph J. Richardson, and Frank Caruso**

ARC Centre of Excellence in Convergent Bio-Nano Science and Technology, and the Department of Chemical Engineering, The University of Melbourne, Parkville, Victoria 3010, Australia

Abstract

Intracellular delivery of proteins is a promising strategy for regulating cellular behavior and therefore has attracted interest for biomedical applications. Despite the emergence of various nanoparticle-based intracellular delivery approaches, it remains challenging to engineer a versatile delivery system capable of responding to various physiological triggers without the need for complex chemical synthesis of the delivery system. Herein, we develop a template-mediated supramolecular assembly strategy to synthesize protein–polyphenol nanoparticles (NPs) capable of endosomal escape and subsequent protein release in the cytosol. These NPs are stable in serum and undergo surface charge reversal from negative to positive in acidic environments, leading to spontaneous endosomal escape. In the cytosol, endogenous small peptides and amino acids with

relatively high charge densities, such as glutathione, trigger NP disassembly through competitive supramolecular interactions, thereby releasing functional bioactive proteins, as validated using cytochrome C and β-galactosidase. The versatility of the present strategy in terms of nanoparticle size, protein type, and functional protein delivery makes this a promising platform for potential application in the field of protein therapeutics.

Keywords: nanoparticle, protein delivery, charge reversal, polyphenol, supramolecular interaction, glutathione

The delivery of proteins to intracellular targets has emerged as an attractive strategy in biomedicine and biotechnology owing to the higher specificity and relatively lower side effects of proteins when compared with genetic or small-molecule therapeutics.[1] However, native proteins generally display limited access to cells, as well as high clearance and low stability in the blood stream, which collectively reduce their potential for efficient intracellular delivery.[2] Conventional approaches for intracellular protein delivery include the chemical modification of proteins with cell-penetrating peptides or other ligands,[3,4] the complexation of cargo proteins with carriers, such as polymers, liposomes, and nanoparticles,[5–7] the genetic engineering of the protein systems themselves, for example with protein transduction domains,[8,9] or membrane disruption methods such as microinjection or electroporation.[10] Among these techniques, polymer-mediated intracellular protein delivery is particularly promising owing to the ease of protein functionalization and the overall effectiveness of intracellular delivery.[6,11,12] For example, cationic polymers have been used as carriers for protein translocation[13] and fluoropolymers have been used to encapsulate proteins for intracellular delivery.[14] However, concerns still remain regarding the

binding affinity of polymers with diverse proteins and the overall safety of some polymer conjugates.[6,13]

Advances in nanotechnology have enabled the development of a number of nanoparticle-based systems that can effectively deliver specific proteins, however, these often involve complex synthesis routes.[15–17] Efficient and versatile intracellular protein delivery requires nanoparticles (NPs) to (i) accommodate various proteins, (ii) be stable in serum, (iii) enter cells and escape endosomal compartments, and (iv) release intact functional proteins in the cytosol.[18] However, few approaches have emerged that can fulfill all of these requirements. Furthermore, an alternative to synthesizing NPs with increasing complexity would be to identify simple and readily available building blocks that are capable of assembling with proteins through various adaptable supramolecular interactions.[19] Previous noncovalent strategies for intracellular delivery have been demonstrated such as those based on the commercially available Chariot peptide (Pep-1, Pep-2) for protein transduction[20] or pyrenebutyrate treatment for membrane translocation of peptides or quantum dots.[21,22] These examples demonstrate the promise of supramolecular interactions for engineering NPs as carriers for the intracellular delivery of native proteins.

We recently reported the templated assembly of microcapsules from various proteins with polyphenols *via* diverse supramolecular interactions and demonstrated that the assembly process did not inhibit the functionality of the proteins.[23] Devising future synthesis strategies based on the identification of suitable NP templates is expected to allow for the formation of protein-based NPs with suitable sizes and functionalities useful for intracellular protein delivery. Herein, three therapeutic proteins (cytochrome C (CYC), immunoglobulin G (IgG), and β-galactosidase (β-Gal)) are examined and assembled with tannic acid (TA) on sacrificial mesoporous silica (MS) NP templates to form protein–polyphenol NPs, which are obtained after template dissolution (Scheme

1a). These protein–TA NPs are stable in both serum-containing media and human plasma for more than 1 week and can be readily internalized in cells. The diameters of the NPs are tunable, as they are determined by the diameters of the template particles. Importantly, the protein–TA NPs can escape endosomal compartments, as acidic environments such as those present in endosomes (pH 4.5–7.0) trigger a surface charge reversal on the NPs.[24] Finally, upon reaching the cytosol, functional protein is released when intracellular glutathione (GSH, 1–11 mM in the cytosol[25]) triggers supramolecular disassembly of the NPs *via* the formation of competitive noncovalent interactions with both the protein and TA (Scheme 1b). Specifically, CYC–TA NPs can induce cell apoptosis after incubation for 48 h and β-Gal–TA NPs can induce catalytic hydrolysis inside cells. This robust protein–TA NP assembly strategy provides opportunities for the development of protein delivery vehicles.

Scheme 1. Supramolecular Assembly of Protein–TA NPs and Intracellular Protein Delivery.

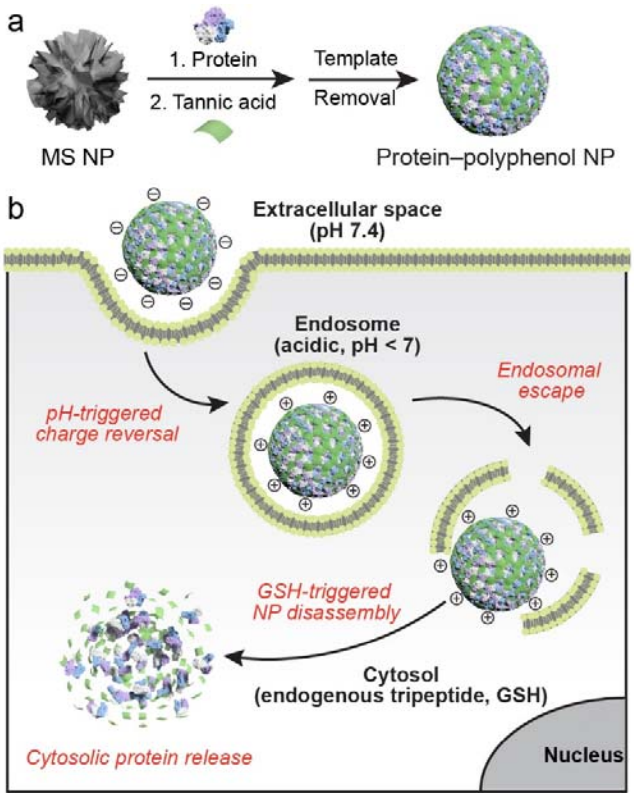

[a]Schematic of the supramolecular assembly of a protein–TA NP on a sacrificial template (mesoporous silica, MS). [b]Scheme depicting intracellular protein delivery from a protein–polyphenol NP.

Results and Discussion

Protein–TA NPs were synthesized *via* the self-assembly of a protein and TA on sacrificial MS NPs (Scheme 1a and Figure S1). First, the protein was incubated with MS NPs for 12 h, and after washing off excess protein, TA was used to "cross-link" the protein *via* noncovalent interactions. Stable protein–polyphenol NPs were obtained after template removal with hydrofluoric acid. CYC was chosen as a model protein for investigating the physicochemical parameters and therapeutic efficacy of the polyphenol–TA NPs because it can only induce cell apoptosis *via* mitochondrial affinity after entering the cytosol.[26] After template removal, CYC–TA NPs in solution displayed a hydrodynamic size distribution similar to that of the MS template (Figure 1a), centered at ~250 nm. Atomic force microscopy (AFM) measurements showed that the CYC–TA NPs were smaller (*i.e.*, ~120 nm) owing to the air-drying process (Figure 1b and Figure S2), suggesting the soft nature of the NPs. A similar degree of shrinkage was observed from both transmission electron microscopy (TEM) and scanning electron microscopy (SEM) analyses (Figure 1c and Figure S3). The UV–vis spectra of the CYC–TA NPs featured the heme group peak at 410 nm, similar to that observed in free CYC (Figure 1d), and the circular dichroism spectra of CYC–TA NPs and free CYC also indicated the preservation of protein structure after assembly (Figure S4). The present strategy was applicable to various proteins of different sizes and isoelectric points (pIs), as exemplified from the successful preparation of IgG–TA NPs and β-Gal–TA NPs (Figure 1e, f). Owing to the higher molecular weights of IgG (~150 kDa, pI 8.0) and β-Gal (~430 kDa, pI 5.0) compared with that of CYC (~12 kDa, pI 9.8),[27] the air-dried IgG–TA NPs and β-Gal–TA NPs displayed denser morphologies and larger diameters (Figure S5), indicating that careful choice of the protein affords tuning of the physical properties of the protein–TA NPs. In addition, the size

of the protein–TA NPs could be varied according to the size of the MS template (Figure S6), allowing for better size control of NPs in contrast with the template-free self-assembly of these similar protein–TA complexes (Figure S7). Collectively, the control afforded by the present strategy *via* tuning of the physicochemical properties of the NPs (*e.g.*, size, density) presents a viable route to modulate the bio–nano interactions of NPs.[28] Importantly, the various structures (tertiary or quaternary) and functional side chains of proteins not only affect the binding ratio of protein and TA (Figure S8) but also govern the different interactions between proteins with TA (Figure S9), which allows for the design of NPs capable of responding to diverse physiological environments.

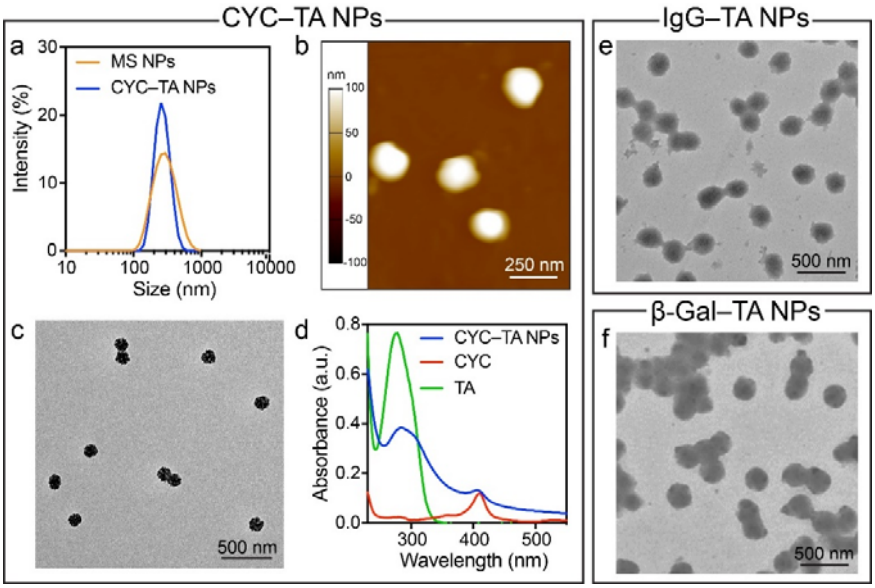

Figure 1. (a) Size distribution profiles of MS NPs (template) and CYC–TA NPs measured in aqueous solution. (b) AFM and (c) TEM analyses of CYC–TA NPs. (d) UV–vis spectra of CYC–TA NPs, CYC, and TA. (e, f) TEM images of IgG–TA and β-Gal–TA NPs.

Figure 2a shows the pH-responsive surface charge reversal nature of the CYC–TA NPs, transitioning from negative to positive as the pH is switched from pH 6 to pH 5. This charge

reversal is likely due to the protonation of a single hydroxyl moiety in each galloyl group as CYC (pI 9.8) is positively charged at the pH values examined (4.5–7.4).[29] Other protein–TA NPs (IgG and β-Gal) also exhibited charge reversal but this occurred at pHs related to their pIs (Figure S10). Negatively charged NPs are considered to perform better (*i.e.*, they display less nonspecific binding and clustering) in the extracellular environment (pH 7.4).[30] In contrast, positively charged materials have a higher tendency to escape the acidic intracellular compartments (pH 4.5–5.5) that internalize NPs.[31] The surface charge of the CYC–TA NPs was negative at pH 7.4, likely due to the presence of the phenolic groups on the surface of the NPs, which conferred colloidal stability to the NPs. As confirmed from the dynamic light scattering (DLS) analysis, aggregation or disassembly of the CYC–TA NPs was not observed following incubation for 192 h in diverse media, *i.e.*, phosphate buffered saline (PBS), Dulbecco's modified Eagle medium (DMEM) with 10% fetal bovine serum (FBS), human plasma, and different pH solutions (Figure 2b, c). To validate endosomal escape of the NPs, fluorescein isothiocyanate (FITC)-labeled CYC–TA NPs were incubated with HeLa cells for 4 or 24 h and their intracellular distribution was examined. Generally, a portion of the internalized CYC–TA NPs were not colocalized with acidic compartments such as the endosomes and lysosomes at 4 h (Figure S11), as indicated from the relatively low Pearson's correlation coefficient R value of 0.28 ± 0.03 (Figure S12), where the R value ranges from 1, when the green and red fluorescence signals are 100% linearly correlated (*i.e.*, colocalization), to 0% when the signals have no correlation (*i.e.*, endosomal escape).[32,33] After 24 h incubation with NPs, the cells displayed diffuse green fluorescence, suggesting both endosomal escape and intracellular disassembly of the NPs (Figure 2d), which are in agreement with electroporation results using free CYC (Figure S13). Additionally, calcein leakage assays of cells treated with CYC–TA NPs confirmed that the NPs could destabilize endo/lysosomal membranes

(Figure S14).[34] In contrast, MS NPs loaded with FITC-CYC did not escape from endosomes even after incubation for 24 h, which demonstrated the important contributions of TA in regards to the endosomal escape of CYC–TA NPs (Figure S15). FITC-labeled IgG–TA NPs also escaped from endo/lysosomes as validated by CLSM images after 4 h (Figure S16). These results suggest that NPs self-assembled from simple and natural building blocks, without complex chemical modification, can successfully escape the endosome, a requirement for intracellular protein release.[35]

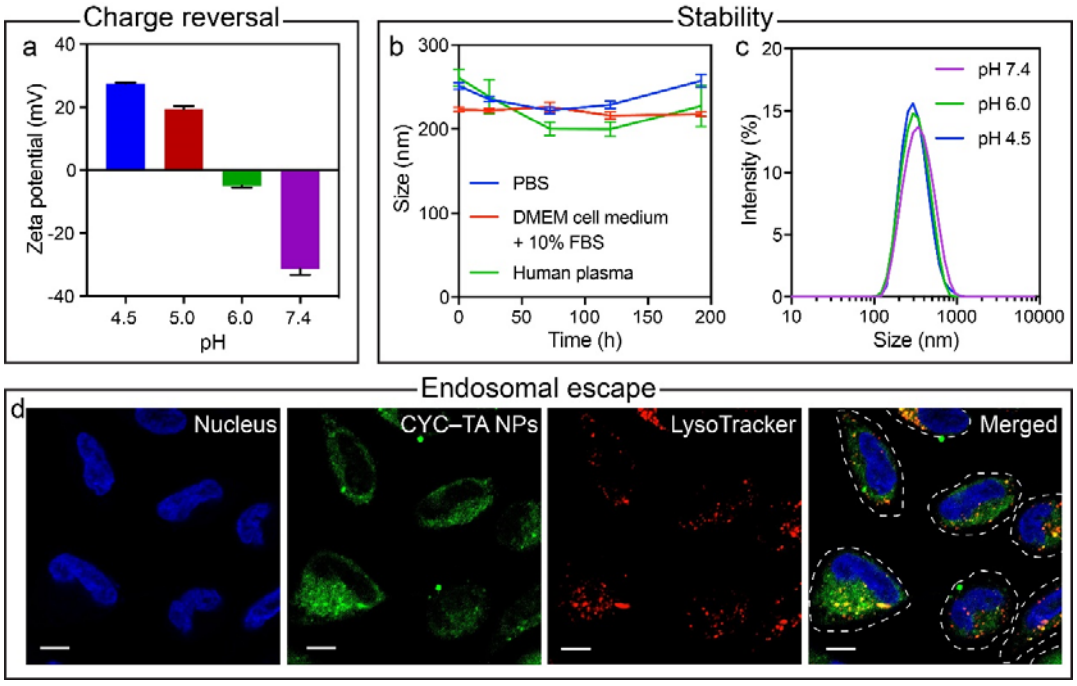

Figure 2. (a) Charge reversal of CYC–TA NPs assessed by microelectrophoresis (*i.e.*, zeta-potential) measurements at different pH. (b) Stability of CYC–TA NPs in different media assessed by monitoring the diameter of the NPs for 192 h by DLS. (c) Size distribution of CYC–TA NPs as a function of pH. (d) Confocal laser scanning microscopy imaging of a LysoTracker colocalization assay performed in HeLa cells after incubation for 24 h with FITC-labeled CYC–TA NPs. Scale bars: 10 μm.

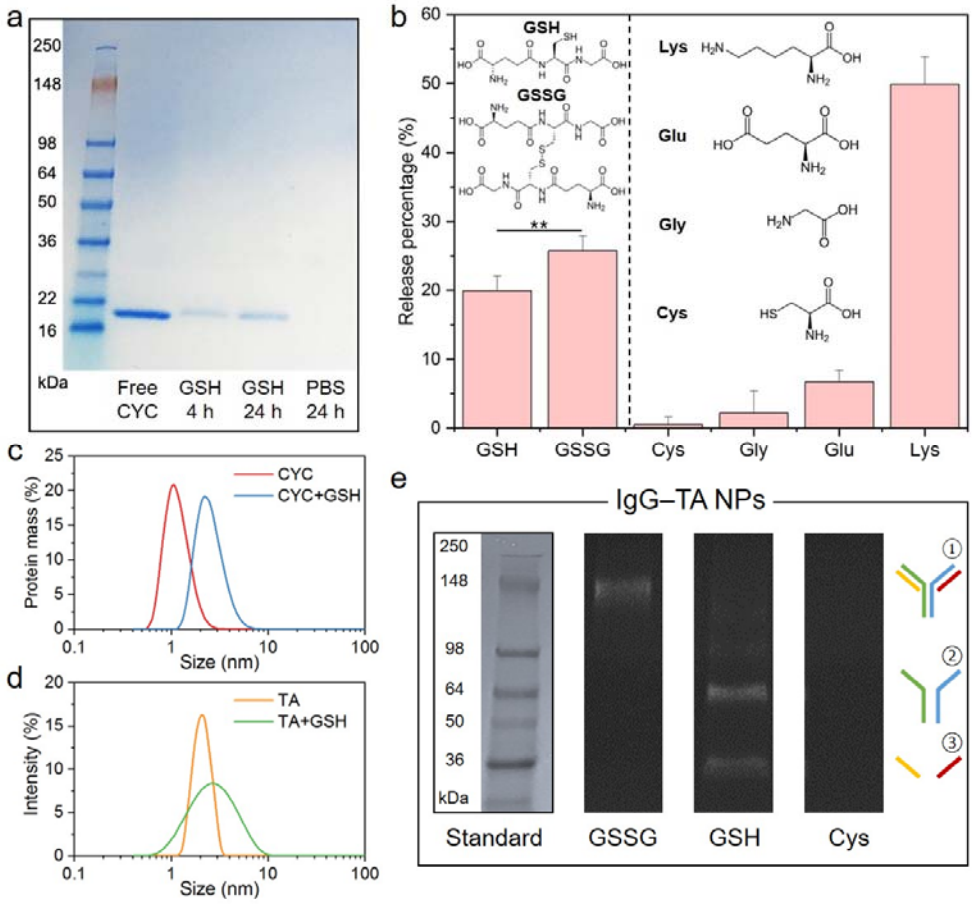

Figure 3. (a) SDS-PAGE analysis of supernatants released from the incubation of CYC–TA NPs with 10 mM GSH for 4 h and 24 h or with 1× PBS for 24 h. The positive control was free CYC. (b) Percentage of CYC released from CYC–TA NPs after incubation for 4 h with GSH (10 mM), GSSG (5 mM), Lys (10 mM), Glu (10 mM), Gly (10 mM), or Cys (10 mM). The corresponding chemical structures are also shown. The experiments were performed in triplicate and expressed as mean ± standard deviation (SD) ($n = 3$). $^{**}P < 0.01$ with 95% confidence level from the unpaired *t*-test. (c, d) Changes in the size distribution profiles of CYC protein or TA molecule after mixing with GSH. [CYC] = 0.5 mg mL^{-1}; [TA] = 0.5 mg mL^{-1}; [GSH] = 10 mM. (e) SDS-PAGE analysis of supernatants released from the incubation of IgG–TA NPs with 5 mM GSSG, 10 mM GSH, or

10 mM Cys for 24 h. The schematic on the right represents the structure of intact IgG (①), two heavy chains (②), and two light chains (③).

We then investigated the release of the proteins from the NPs in the intracellular environment after endosomal escape. It was postulated that the noncovalent (supramolecular assembly)[23] and charge-shifting nature of the NPs may trigger, through competitive binding with cytosolic proteins, the release of the protein CYC. Because the NPs have been shown to be stable in various protein-containing media (Figure 2b), the trigger is expected to be a protein or peptide not readily present in the extracellular or endosomal environment. The cytosol contains GSH, present at a high concentration (1–11 mM),[25] which is widely used as a representative intracellular component to stimulate the disassembly of disulfide-based NPs *via* cleavage of the cross-linker.[26,36] Particularly, owing to its zwitterionic nature, GSH can interact with both the positively charged CYC and negatively charged TA to instigate the disassembly of the protein NPs. To investigate this hypothesis, CYC–TA NPs were incubated with GSH (10 mM) for 4 and 24 h and sodium dodecyl sulfate and polyacrylamide gel electrophoresis (SDS-PAGE) was performed. The findings revealed that CYC was gradually released from the NPs (following incubation for 24 h), which was not observed upon incubation in PBS (control) (Figure 3a and Figure S17). Additionally, lower concentrations of GSH (1 and 5 mM) can still induce the disassembly of NPs and gradual protein release (Figure S18). To examine the GSH-triggered release mechanism, CYC–TA NPs were treated for 4 h with GSH (10 mM), oxidized glutathione (GSSG, 5 mM), and individual amino acids (*i.e.*, glutamic acid (Glu), cysteine (Cys), glycine (Gly), lysine (Lys); 10 mM). The highest concentration at which GSH is found in the cytosol is ~10 mM.[37–39] To ensure that the molar content of the functional groups in GSSG and GSH is the same, a concentration of 5 mM was chosen for GSSG. The concentration of the amino acids was chosen to match that of GSH.

The protein release amounts measured by the UV–vis absorbance at 410 nm demonstrated that GSSG triggered a slightly higher CYC release (~25%) than GSH (~20%) (Figure 3b and Figure S19). The individual amino acids composing GSH released far less CYC, with Glu releasing ~6% CYC, followed by Gly (~2%) and Cys (~0.2%). In contrast, the positively charged Lys, which features a flexible and long side-chain and has more amino groups than GSH or the other individual amino acids (*i.e.*, 2 in Lys *vs* 1 each in GSH, Gly, and Cys), triggered the most efficient CYC release (~50%) among the different molecules examined (Figure 3b). These results suggest that multiple carboxyl and amine groups may act as important triggering sites rather than the thiol groups of GSH, which is typically used to trigger the intracellular destabilization of nanocarriers.[39,40] The multiple binding moieties of GSH and GSSG can offer multivalent interactions with a single CYC or TA that are collectively stronger than the corresponding monovalent interactions from individual amino acids.[41] In addition, serum proteins such as FBS with globular structures and low charge densities only formed a protein corona around the surface of the NPs in comparison to the disassembly of the NPs caused by GSH and GSSG, as assessed by DLS (Figure S20). This suggests that intracellular disassembly of the NPs is triggered by endogenous small peptides and amino acids.

CYC contains several lysine and arginine moieties (~18% of total amino acids) that are positively charged at physiological pH and readily accessible on the surface of the protein (Figure S21). Both lysine and arginine can complex with the carboxylate ions in GSH by forming salt bridges, a combination of hydrogen bonding and ionic interactions.[42–45] After the addition of GSH to a solution of free CYC, the size of CYC (assessed by relative mass composition distribution) increased by an order of magnitude (due to aggregation) relative to the size of free CYC (Figure 3c). This result suggests that competitive binding with CYC is one possible mechanism for protein

release from the NPs (Figure S22).[46] However, GSH can also form noncovalent interactions (ionic interactions *via* the N-terminus or hydrogen bonding *via* the amide backbone and C-terminus) with TA, leading to molecular clustering as measured by DLS (Figure 3d), which suggests that this GSH-triggered protein release may be applicable to other protein–TA NPs.

IgG–TA NPs also demonstrated GSH/GSSG-triggered NP disassembly and protein release (Figure 3e). Intact IgG was released from the IgG–TA NPs following incubation with GSSG, whereas incubation with GSH led to IgG release and fragmentation into heavy and light chains *via* disulfide cleavage. Incubation with Lys also led to the release of intact IgG, whereas Cys could not induce significant protein release, further demonstrating that the presence of multivalent charges is more important than the presence of reducing conditions (Figure S23). Collectively, these results demonstrate that the dual-responsive endosomal escape and intracellular delivery achieved herein is an attribute of the delivery platform itself, rather than specific protein–polyphenol pairing.

The bioactivity of the protein released from the NPs was then evaluated. The apoptotic activity of CYC was first monitored by flow cytometry using an annexin V and propidium iodide (PI) staining kit. The results showed that CYC–TA NPs induced ~12% early apoptosis and ~10% late apoptosis toward model Jurkat cells (human T-cell leukemia cell line) after 48 h (Figure 4a, b) owing to the low nonspecific association of T cells with NPs (~30% cells were associated with NPs after 48 h, Figure S24). Furthermore, the cell viability results revealed that the CYC–TA NPs could cause cell death in two different breast cancer cell lines, MDA-MB-231 and BT-474, after 48 h of incubation (Figure 4c and Figure S25), demonstrating general cytotoxic effects for different types of cells including suspension and adherent cells. In contrast, free CYC showed negligible cell toxicity due to a lack of uptake or trafficking to the cytosol. Note that the effective CYC

concentrations (5–100 μg mL^{-1}) for our CYC–TA NPs to induce apoptosis are consistent with other literature reports of NP systems capable of escaping the endosome and delivering CYC to the cytosol.[26,47] In addition, NPs composed of a non-toxic protein (IgG–TA NPs) also displayed negligible cytotoxicity toward both cancer cell types (Figure 4c and Figure S25) and were not capable of inducing cell apoptosis in Jurkat cells (Figure S26), highlighting the tunable, high biocompatibility of polyphenol-based NPs.

To confirm that the activity of the proteins was also maintained in other protein–polyphenol NPs, β-Gal–TA NPs were also studied. MDA-MB-231 cells were treated with β-Gal–TA NPs followed by the addition of 5-bromo-4-chloro-3-indolyl-β-D-galactoside (X-Gal). β-Gal catalyzes the hydrolysis of X-Gal into an insoluble blue dye, which can be used to determine the amount of bioactive β-Gal in the treated cells.[48] As observed from the results in Figure 4d, incubation of β-Gal–TA NPs with the cells resulted in a high accumulation of blue dye in the cells after X-Gal staining, confirming the intracellular delivery of active protein. Moreover, the cell targeting ability of the antibodies in the NPs was evaluated using an anti-CD44 antibody that can specifically target CD44-overexpressing cells (MDA-MB-231).[49] The anti-CD44–TA NPs showed high binding specificity toward MDA-MB-231 cells (46% cell association after 4 h) compared with the negative control of IgG–TA NPs (3% cell association after 4 h) (Figure S27), demonstrating preservation of the antibody function after NP assembly. To improve reproducibility, reporting, and re-analysis, this study conforms to the Minimum Information Reporting in Bio–Nano Experimental Literature (MIRIBEL) standard,[50] and a companion checklist is provided in the Supporting Information.

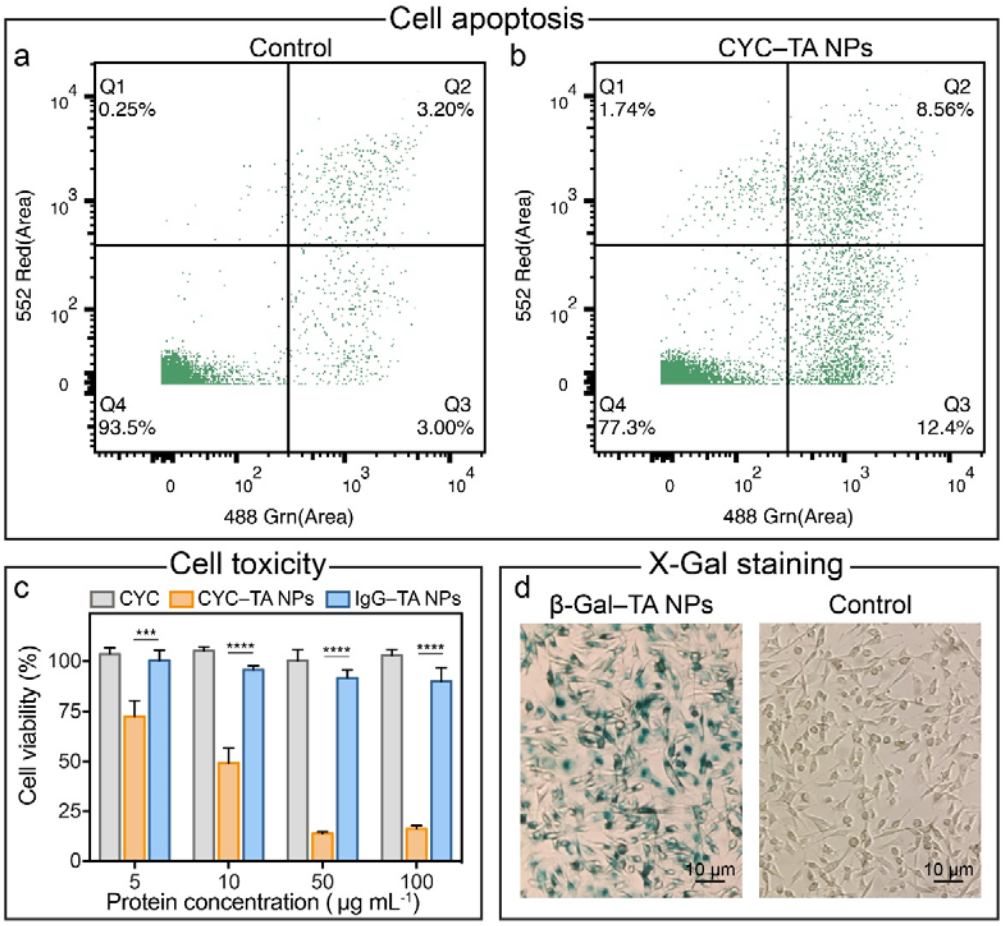

Figure 4. (a, b) Cell apoptosis assay by annexin V-FITC/PI staining performed on Jurkat cells that were incubated in the absence (Control) or presence of CYC–TA NPs for 48 h at 37 °C. Q1–Q4 represent necrotic cells, late apoptotic cells, early apoptotic cells, and live cells, respectively. (c) Cell viability of MDA-MB-231 cells incubated in the presence of free CYC, CYC–TA NPs, or IgG–TA NPs at different protein dosages for 48 h at 37 °C. (Data are shown as the mean ± SD, $n = 6$, ***$P < 0.001$, ****$P < 0.0001$ from the unpaired t-test). (d) X-Gal staining of MDA-MB-231 cells treated with β-Gal–TA NPs for 24 h. The control group was treated with free β-Gal.

Conclusions

In summary, we have developed a versatile strategy for the intracellular release of proteins in response to multiple endogenous triggers. These supramolecular protein–TA NPs are stable in the extracellular environment but rapidly disassemble in the cytosol of cells due to competitive binding of small intracellular peptides such as GSH or GSSG. Importantly, the protein–TA NPs can escape the endosome after internalization through intrinsic charge shifting in acidic environments. The released proteins, *i.e.*, CYC or β-Gal, maintain their bioactivity after intracellular delivery. This simple and general strategy allows for protein delivery and is thus promising for a variety of therapeutic applications. Owing to the universal adhesion properties of polyphenols,[51,52] it is expected that other cargo, such as DNA and RNA,[53] could also be formulated with the NPs for therapeutic co-delivery.

Experimental Section

Materials. TA, PBS, glycine, hydrogen chloride (HCl), FITC, CYC, IgG, β-Gal, GSH, GSSG, Glu, Cys, Gly, Lys, ethylene glycol-bis(2-aminoethylether)-*N*,*N*,*N*′,*N*′-tetraacetic acid (EGTA), magnesium chloride ($MgCl_2$), glutaraldehyde, potassium ferrocyanide ($K_4Fe(CN)_6 \cdot 3H_2O$), potassium ferricyanide ($K_3Fe(CN)_6$), cetyltrimethylammonium bromide (CTAB), sodium salicylate (NaSal), tetraethyl orthosilicate (TEOS), and triethylamine (TEA) were purchased from Sigma-Aldrich. DMEM, Roswell Park Memorial Institute (RPMI) 1640 medium, FBS, and Dulbecco's phosphate-buffered saline (DPBS) were obtained from Life Technologies. SimplyBlue™ SafeStain, NuPAGE LDS sample buffer (4×), and SeeBlue™ Plus2 pre-stained protein standard were purchased from Invitrogen. Mini-PROTEAN TGX precast gels and Tris/Glycine/SDS running buffer (10×) were purchased from Bio-RAD. High-purity Milli-Q water

with a resistivity of 18.2 MΩ cm was obtained from an inline Millipore RiOs/Origin water purification system.

Characterization. TEM of the particles were performed on an FEI Tecnai TF20 instrument (USA) at an operation voltage of 200 kV. The TEM samples were prepared by dropping an aliquot (5 μL) of diluted samples (~0.05 mg mL^{-1}) on formvar carbon-coated copper grids. SEM images of the particles were captured on an FEI Quanta 200 field-emission scanning electron microscope, operating at an accelerating voltage of 10 kV. For the SEM experiments, dried samples (gold-sputtered) were used. AFM experiments were conducted on an Asylum Research Cypher AFM instrument. Optical microscopy images of X-Gal-stained cells were acquired on an inverted Olympus IX71 microscope. Confocal laser scanning microscopy (CLSM) images were captured on a Nikon A1R+ confocal laser scanning microscope (Nikon Corporation, Japan). UV–Visible absorption spectra were recorded on a Specord 250 Plus spectrophotometer (Analytik Jena AG). Size and surface zeta potential measurements of the particles were performed in water and in different pH buffers at a concentration of 5 mM on a Malvern Zetasizer Nano ZS instrument (Malvern Instrument, Worcestershire, UK). Protein molecular size (assessed by relative mass composition distribution) and TA molecular size (assessed by intensity distribution) measurements were performed on this Zetasizer. Circular dichroism spectra were recorded on a Model 410 circular dichroism spectrometer (Aviv Biomedical, Inc.).

Cell Culture. HeLa, Jurkat, MDA-MB-231, and BT-474 cells were purchased from the American Type Culture Collection (USA). HeLa, MDA-MB-231, and BT-474 cells were maintained in complete DMEM media containing 10% FBS. Jurkat cells were maintained in complete RPMI-1640 medium supplemented with 10% FBS. All cell lines were maintained at 37 °C in a cell culture incubator with 5% CO_2 and 95% relative humidity.

Synthesis of MS Particle Templates. MS templates with large and interconnected pores were synthesized by the anion-assisted method and modified from the literature.[54] Briefly, TEA (68 mg, catalyst), CTAB (380 mg, cationic surfactant), and NaSal (168 mg, structure-directing agent) were successively added to Milli-Q water (25 mL) in a round-bottom flask, and the solution mixture was stirred at 80 °C in an oil bath for 1 h. Then, TEOS (4 mL, silica source) was added dropwise to the above mixture within 10 s and this solution was stirred (175 *g*) at 80 °C for 2 h. The reaction products were washed with ethanol three times and then purified three times by extraction with 1 M HCl in methanol at 60 °C for 6 h. The MS template particles were finally oven-dried at 80 °C overnight for future use.

Synthesis of Protein–TA NPs. Protein (50 μL, 10 mg mL^{-1}) was added to an aqueous MS particle solution (200 μL, 10 mg mL^{-1}). The resulting suspension was vigorously mixed in an ultrasonic bath for 2 min and then incubated in an Eppendorf thermomixer overnight at 37 °C and 1400 rpm. The particles were washed with Milli-Q water once to remove excess protein and resuspended in Milli-Q water (200 μL), after which an aliquot (5 μL) of TA (40 mg mL^{-1}) was added to the particle solution. The resulting suspension was vigorously mixed in an ultrasonic bath for 2 min and then incubated in an Eppendorf thermomixer at 37 °C and 1400 rpm for 4 h. The particles were retrieved and washed with Milli-Q water three times to remove excess TA. In the washing step, the particles were spun down by centrifugation (4000 *g*, 5 min) and the supernatant was removed. The particles were then resuspended with vigorous mixing prior to the next wash step. Protein–TA NPs were obtained after removal of the MS template with a 1 M HF/3 M NH_4F solution (pH ~5).[55] *Caution! HF is highly toxic and only small quantities should be prepared and handled with extreme care.* The resultant protein–TA NPs were washed three times with water and resuspended in water.

Extracellular Stability of Protein–TA NPs. The extracellular stability of the CYC–TA NPs was examined by monitoring changes in the particle size over 192 h using DLS. The samples were incubated in 1× PBS, DMEM cell medium+10% FBS, or human plasma before being subjected to the DLS measurements. The experiments were performed in triplicate and the results are expressed as mean ± SD (n = 3).

Endosomal Escape of Protein–TA NPs. HeLa cells were seeded into 8-well Lab-Tek chambered coverglass slides (Thermo Fisher Scientific, USA) at a cell density of 4×10^4 cells per well and then cultured in complete media at 37 °C for 24 h to allow cellular adhesion on substrates. Then, FITC-labeled CYC–TA NPs were added to the cells at a protein concentration of 50 μg mL^{-1} and then incubated for 4 h or 24 h at 37 °C. After incubation, the treated cells were gently washed three times with DPBS and stained with LysoTracker® Red for endosome/lysosome labeling, and the colocalization of the green and red fluorescence signals were studied. Live cell imaging was performed by CLSM using a Plan Apo λ 60× 1.4 NA oil immersion objective, 405, 488, 561, and 640 nm lasers, and 450/50, 525/50, 595/50, and 700/75 nm bandpass emission filters. The images were processed by Fiji software.

Calcein Leakage Assay. MDA-MB-231 cells were seeded in 8-well Lab-Tek chambered coverglass slides (Thermo Fisher Scientific, USA) at a cell density of 4×10^4 cells per well in complete media (400 μL) at 37 °C for 24 h to allow cellular adhesion on substrates. Then, the culture media was aspirated and replaced with fresh media (180 μL), and calcein (20 μL, 1.5 mg mL^{-1} in DPBS) was added to each well in the presence or absence of NPs at a protein centration of 50 μg mL^{-1} and incubated with cells for 4 h. Nonfluorescent CYC–TA NPs were used in this assay to avoid interference with the calcein signal. After incubation, the treated cells were gently washed four times with DPBS and live cells were imaged by CLSM.

Release Studies of Protein–TA NPs Assessed by SDS-PAGE. For the protein release studies, the protein–TA NPs were incubated with 10 mM GSH, 5 mM GSSG, or 1× PBS at 37 °C for a designated time. Centrifugation (5000 *g*, 10 min) was then performed to remove the intact NPs and complexes before subjecting the supernatants to polyacrylamide gel electrophoresis. Aliquots (15 μL) of the supernatants containing the released proteins were mixed with NuPAGE LDS sample buffer (5 μL, 4×), after which aliquots (18 μL) of the samples were loaded into the gel lanes. The gel was run using 1× Tris/Glycine/SDS running buffer at 200 V until the dye front reached the reference line. Then, the gels were stained with SimplyBlue™ SafeStain for 1 h under mild shaking and washed with water for at least 1 h to visualize protein staining. The stain-free gels were activated in the stain-free-enabled imager (Gel Doc, BIO-RAD).

Cytotoxicity Assay of CYC–TA NPs. The (sodium 3′-[1-(phenylaminocarbonyl)-3,4-tetrazolium]-bis(4-methoxy-6-nitro) benzene sulfonic acid hydrate) (XTT)-based *in vitro* cytotoxicity assay was performed to assess the biocompatibility of the protein–TA NPs. XTT was dissolved in complete DMEM (with 10% FBS) to form a 0.2 mg mL^{-1} solution, and phenazine methosulfate (PMS) was dissolved in DPBS to form a 1 mM solution. The XTT reagent was activated by mixing with PMS solution at a volume ratio of 400:1. MDA-MB-231 and BT-474 cells were seeded on a 96-well plate at a cell density of 2×10^4 cells per well and cultured in complete DMEM media at 37 °C for 24 h to allow cellular adhesion on substrates. After incubation with the CYC–TA NPs or free CYC at various protein concentrations for 48 h, the media in the 96-well plate was aspirated and replaced with fresh activated XTT media (100 μL). The cells were further incubated for 4 h and the absorbance at 475 nm was measured relative to non-treated cells. The experiments were performed in sextuplicate and the results are expressed as mean ± SD (n = 6).

Cell Apoptosis with CYC–TA NPs. Jurkat cells were seeded on a 6-well plate at a cell density of 10×10^4 cells per well and cultured in complete media at 37 °C. CYC–TA NPs at a protein centration of 50 μg mL^{-1} were added to the cell medium and incubated for 24 h. The cells were harvested after the incubation period and washed in cold PBS buffer. The washed cells were then resuspended in 1× annexin-binding buffer (100 μL). Aliquots of Alexa Fluor® 488 annexin V (5 μL) and PI working solution (1 μL) were added to the cell suspension (100 μL) and the cells were incubated at room temperature for 15 min. After the incubation period, 1× annexin-binding buffer (400 μL) was added to the sample and the stained cells were analyzed by flow cytometry by measuring the fluorescence emission at 530 nm and 575 nm using 488 nm excitation.

X-Gal Staining for Intracellular Delivery of β-Gal. MDA-MB-231 cells were treated with β-Gal–TA NPs for 24 h. Then, the cell media was aspirated off and the treated cells were fixed with X-Gal fix buffer (100 mM phosphate buffer (pH 7.4) supplemented with 5 mM EGTA, pH 7.3, 2 mM $MgCl_2$ and 0.2% glutaraldehyde) for 15 min at room temperature. The cells were washed twice (5 min each) with X-Gal wash buffer (100 mM phosphate buffer (pH 7.4) supplemented with 2 mM $MgCl_2$) and incubated with the X-Gal staining buffer (100 mM phosphate buffer (pH 7.4) supplemented with 2 mM $MgCl_2$, 5 mM $K_4Fe(CN)_6$, and 5 mM $K_3Fe(CN)_6$) containing 1 mg mL^{-1} X-Gal overnight at 37 °C inside an enclosed humidified chamber. The treated cells were further washed with X-Gal wash buffer and observed under an optical microscope.

MIRIBEL. The studies conducted herein, including material characterization, biological characterization, and experimental details, conform to the MIRIBEL reporting standard for bio–nano research,[50] and we include a companion checklist of these components herein.

ASSOCIATED CONTENT

Supporting Information. TEM image of SiO_2 particles, AFM and SEM images of CYC–TA NPs, CD spectra of CYC–TA NPs, size distribution of air-dried protein–TA NPs, mass/molar ratio of TA and proteins inside NPs, interaction-dependent disassembly of protein–TA NPs, charge reversal of protein–TA NPs, CLSM images and corresponding Pearson's *R* values for endosomal escape, original SDS-PAGE of released protein solutions, cell viability, cell targeting of antibody–TA NPs, and MIRIBEL checklist for reporting research in bio–nano science. This material is available free of charge *via* the Internet at http://pubs.acs.org.

AUTHOR INFORMATION

Corresponding Author

Frank Caruso. E-mail address fcaruso@unimelb.edu.au

ACKNOWLEDGMENT

This research was conducted and funded by the Australian Research Council Centre of Excellence in Convergent Bio-Nano Science and Technology (project number CE140100036). F.C. acknowledges the award of a National Health and Medical Research Council Senior Principal Research Fellowship (GNT1135806). This work was performed in part at the Materials Characterisation and Fabrication Platform and the Bio21 Advanced Microscopy Facility at The University of Melbourne and the Victorian Node of the Australian National Fabrication Facility. We thank Dr. René Lafleur, Dr. Christina Cortez-Jugo, Denzil Furtado, and Agata Glab for helpful discussions and Paula Cevaal, Dr. Yi Ju, Jingqu Chen, Yijiao Qu, and Jiaying Song for assistance with experiments.

References

1. Stewart, M. P.; Sharei, A.; Ding, X.; Sahay, G.; Langer, R.; Jensen, K. F. *In Vitro* and e*x Vivo* Strategies for Intracellular Delivery. *Nature* **2016**, *538*, 183–192.
2. Gu, Z.; Biswas, A.; Zhao, M.; Tang, Y. Tailoring Nanocarriers for Intracellular Protein Delivery. *Chem. Soc. Rev.* **2011**, *40*, 3638–3655.
3. Fu, J.; Yu, C.; Li, L.; Yao, S. Q. Intracellular Delivery of Functional Proteins and Native Drugs by Cell-Penetrating Poly(disulfide)s. *J. Am. Chem. Soc.* **2015**, *137*, 12153–12160.
4. Mix, K. A.; Lomax, J. E.; Raines, R. T. Cytosolic Delivery of Proteins by Bioreversible Esterification. *J. Am. Chem. Soc.* **2017**, *139*, 14396–14398.
5. Scaletti, F.; Hardie, J.; Lee, Y. W.; Luther, D. C.; Ray, M.; Rotello, V. M. Protein Delivery into Cells Using Inorganic Nanoparticle–Protein Supramolecular Assemblies. *Chem. Soc. Rev.* **2018**, *47*, 3421–3432.
6. Chang, H.; Lv, J.; Gao, X.; Wang, X.; Wang, H.; Chen, H.; He, X.; Li, L.; Cheng, Y. Rational Design of a Polymer with Robust Efficacy for Intracellular Protein and Peptide Delivery. *Nano Lett.* **2017**, *17*, 1678–1684.
7. Vila-Caballer, M.; Codolo, G.; Munari, F.; Malfanti, A.; Fassan, M.; Rugge, M.; Balasso, A.; de Bernard, M.; Salmaso, S. A pH-Sensitive Stearoyl-PEG-Poly(methacryloyl Sulfadimethoxine)-Decorated Liposome System for Protein Delivery: An Application for Bladder Cancer Treatment. *J. Controlled Release* **2016**, *238*, 31–42.
8. Schwarze, S. R.; Ho, A.; Vocero-Akbani, A.; Dowdy, S. F. *In Vivo* Protein Transduction: Delivery of a Biologically Active Protein into the Mouse. *Science* **1999**, *285*, 1569–1572.
9. Schwarze, S. R.; Hruska, K. A.; Dowdy, S. F. Protein Transduction: Unrestricted Delivery into All Cells? *Trends Cell Biol.* **2000**, *10*, 290–295.
10. Stewart, M. P.; Langer, R.; Jensen, K. F. Intracellular Delivery by Membrane Disruption: Mechanisms, Strategies, and Concepts. *Chem. Rev.* **2018**, *118*, 7409–7531
11. Lee, K. Y.; Yuk, S. H. Polymeric Protein Delivery Systems. *Prog. Polym. Sci.* **2007**, *32*, 669–697.
12. Lv, J.; Fan, Q.; Wang, H.; Cheng, Y. Polymers for Cytosolic Protein Delivery. *Biomaterials* **2019**, *218*, 119358.
13. Samal, S. K.; Dash, M.; Van Vlierberghe, S.; Kaplan, D. L.; Chiellini, E.; Van Blitterswijk, C.; Moroni, L.; Dubruel, P. Cationic Polymers and Their Therapeutic Potential. *Chem. Soc. Rev.* **2012**, *41*, 7147–7194.
14. Zhang, Z.; Shen, W.; Ling, J.; Yan, Y.; Hu, J.; Cheng, Y. The Fluorination Effect of Fluoroamphiphiles in Cytosolic Protein Delivery. *Nat. Commun.* **2018**, *9*, 1–8.
15. Spicer, C. D.; Jumeaux, C.; Gupta, B.; Stevens, M. M. Peptide and Protein Nanoparticle Conjugates: Versatile Platforms for Biomedical Applications. *Chem. Soc. Rev.* **2018**, *47*, 3574–3620.
16. Yu, X.; Gou, X.; Wu, P.; Han, L.; Tian, D.; Du, F.; Chen, Z.; Liu, F.; Deng, G.; Chen, A. T.; Ma, C.; Liu, J.; Hashmi, S. M.; Guo, X.; Wang, X.; Zhao, H.; Liu, X.; Zhu, X.; Sheth, K.; Chen, Q.; *et al*. Activatable Protein Nanoparticles for Targeted Delivery of Therapeutic Peptides. *Adv. Mater.* **2018**, *30*, e1705383.
17. Qin, X.; Yu, C.; Wei, J.; Li, L.; Zhang, C.; Wu, Q.; Liu, J.; Yao, S. Q.; Huang, W. Rational Design of Nanocarriers for Intracellular Protein Delivery. *Adv. Mater.* **2019**, *31*, e1902791.
18. Lee, Y. W.; Luther, D. C.; Goswami, R.; Jeon, T.; Clark, V.; Elia, J.; Gopalakrishnan, S.; Rotello, V. M. Direct Cytosolic Delivery of Proteins through Coengineering of Proteins and Polymeric Delivery Vehicles. *J. Am. Chem. Soc.* **2020**, *142*, 4349–4355.

19. Bai, Y.; Luo, Q.; Liu, J. Protein Self-Assembly *via* Supramolecular Strategies. *Chem. Soc. Rev.* **2016**, *45*, 2756–2767.
20. Gros, E.; Deshayes, S.; Morris, M. C.; Aldrian-Herrada, G.; Depollier, J.; Heitz, F.; Divita, G. A Non-Covalent Peptide-Based Strategy for Protein and Peptide Nucleic Acid Transduction. *Biochim. Biophys. Acta, Biomembr.* **2006**, *1758*, 384–393.
21. Jablonski, A. E.; Kawakami, T.; Ting, A. Y.; Payne, C. K. Pyrenebutyrate Leads to Cellular Binding, Not Intracellular Delivery, of Polyarginine Quantum Dots. *J. Phys. Chem. Lett.* **2010**, *1*, 1312–1315.
22. Takeuchi, T.; Kosuge, M.; Tadokoro, A.; Sugiura, Y.; Nishi, M.; Kawata, M.; Sakai, N.; Matile, S.; Futaki, S. Direct and Rapid Cytosolic Delivery Using Cell-Penetrating Peptides Mediated by Pyrenebutyrate. *ACS Chem. Biol.* **2006**, *1*, 299–303.
23. Han, Y.; Lin, Z.; Zhou, J.; Yun, G.; Guo, R.; Richardson, J. J.; Caruso, F. Polyphenol-Mediated Assembly of Proteins for Engineering Functional Materials. *Angew. Chem. Int. Ed.* **2020**,*59*, 15618–15625.
24. Becker, A. L.; Johnston, A. P.; Caruso, F. Layer-By-Layer-Assembled Capsules and Films for Therapeutic Delivery. *Small* **2010**, *6*, 1836–1852.
25. Such, G. K.; Yan, Y.; Johnston, A. P.; Gunawan, S. T.; Caruso, F. Interfacing Materials Science and Biology for Drug Carrier Design. *Adv. Mater.* **2015**, *27*, 2278–2297.
26. Dutta, K.; Hu, D.; Zhao, B.; Ribbe, A. E.; Zhuang, J.; Thayumanavan, S. Templated Self-Assembly of a Covalent Polymer Network for Intracellular Protein Delivery and Traceless Release. *J. Am. Chem. Soc.* **2017**, *139*, 5676–5679.
27. Righetti, P. G.; Tudor, G.; Ek, K. Isoelectric Points and Molecular Weights of Proteins: A New Table. *J. Chromatogr. A* **1981**, *220*, 115–194.
28. Björnmalm, M.; Cui, J.; Bertleff-Zieschang, N.; Song, D.; Faria, M.; Rahim, M. A.; Caruso, F. Nanoengineering Particles through Template Assembly. *Chem. Mater.* **2017**, *29*, 289–306.
29. Vinu, A.; Murugesan, V.; Tangermann, O.; Hartmann, M. Adsorption of Cytochrome C on Mesoporous Molecular Sieves: Influence of pH, Pore Diameter, and Aluminum Incorporation. *Chem. Mater.* **2004**, *16*, 3056–3065.
30. Verma, A.; Stellacci, F. Effect of Surface Properties on Nanoparticle–Cell Interactions. *Small* **2010**, *6*, 12–21.
31. Casey, J. R.; Grinstein, S.; Orlowski, J. Sensors and Regulators of Intracellular pH. *Nat. Rev. Mol. Cell Biol.* **2010**, *11*, 50–61.
32. Chen, J.; Li, J.; Zhou, J.; Lin, Z.; Cavalieri, F.; Czuba-Wojnilowicz, E.; Hu, Y.; Glab, A.; Ju, Y.; Richardson, J. J. Metal–Phenolic Coatings as a Platform to Trigger Endosomal Escape of Nanoparticles. *ACS Nano* **2019**, *13*, 11653–11664.
33. Dunn, K. W.; Kamocka, M. M.; McDonald, J. H. A Practical Guide to Evaluating Colocalization in Biological Microscopy. *Am. J. Physiol.* **2011**, *300*, 723–742.
34. Selby, L. I.; Cortez-Jugo, C. M.; Such, G. K.; Johnston, A. P. Nanoescapology: Progress toward Understanding the Endosomal Escape of Polymeric Nanoparticles. *Wiley Interdiscip. Rev.: Nanomed. Nanobiotechnol.* **2017**, *9*, e1452.
35. Zhang, M.; Chen, X.; Li, C.; Shen, X. Charge-Reversal Nanocarriers: An Emerging Paradigm for Smart Cancer Nanomedicine. *J. Controlled Release* **2020**, *319*, 46–62.
36. Quinn, J. F.; Whittaker, M. R.; Davis, T. P. Glutathione Responsive Polymers and Their Application in Drug Delivery Systems. *Polym. Chem.* **2017**, *8*, 97–126.
37. Meister, A. Glutathione Metabolism and Its Selective Modification. *J. Biol. Chem.* **1988**, *263*, 17205–17208.

38. Zhu, X.; Tang, R.; Wang, S.; Chen, X.; Hu, J.; Lei, C.; Huang, Y.; Wang, H.; Nie, Z.; Yao, S. Protein@Inorganic Nanodumpling System for High-Loading Protein Delivery with Activatable Fluorescence and Magnetic Resonance Bimodal Imaging Capabilities. *ACS Nano* **2020**, *14*, 2172–2182.
39. Chen, D.; Zhang, G.; Li, R.; Guan, M.; Wang, X.; Zou, T.; Zhang, Y.; Wang, C.; Shu, C.; Hong, H.; Wan, L. J. Biodegradable, Hydrogen Peroxide, and Glutathione Dual Responsive Nanoparticles for Potential Programmable Paclitaxel Release. *J. Am. Chem. Soc.* **2018**, *140*, 7373–7376.
40. Cheng, R.; Feng, F.; Meng, F.; Deng, C.; Feijen, J.; Zhong, Z. Glutathione-Responsive Nano-Vehicles as a Promising Platform for Targeted Intracellular Drug and Gene Delivery. *J. Controlled Release* **2011**, *152*, 2–12.
41. Mogaki, R.; Hashim, P. K.; Okuro, K.; Aida, T. Guanidinium-Based "Molecular Glues" for Modulation of Biomolecular Functions. *Chem. Soc. Rev.* **2017**, *46*, 6480–6491.
42. Tang, R.; Kim, C. S.; Solfiell, D. J.; Rana, S.; Mout, R.; Velázquez-Delgado, E. M.; Chompoosor, A.; Jeong, Y.; Yan, B.; Zhu, Z.-J. Direct Delivery of Functional Proteins and Enzymes to the Cytosol Using Nanoparticle-Stabilized Nanocapsules. *ACS Nano* **2013**, *7*, 6667–6673.
43. Mogaki, R.; Okuro, K.; Ueki, R.; Sando, S.; Aida, T. Molecular Glue That Spatiotemporally Turns on Protein–Protein Interactions. *J. Am. Chem. Soc.* **2019**, *141*, 8035–8040.
44. Lv, J.; Tan, E.; Wang, Y.; Fan, Q.; Yu, J.; Cheng, Y. Tailoring Guanidyl-Rich Polymers for Efficient Cytosolic Protein Delivery. *J. Controlled Release* **2020**, *320*, 412–420.
45. Yang, X. C.; Samanta, B.; Agasti, S. S.; Jeong, Y.; Zhu, Z. J.; Rana, S.; Miranda, O. R.; Rotello, V. M. Drug Delivery Using Nanoparticle-Stabilized Nanocapsules. *Angew. Chem. Int. Ed.* **2011**, *50*, 477–481.
46. Raghupathi, K. R.; Guo, J.; Munkhbat, O.; Rangadurai, P.; Thayumanavan, S. Supramolecular Disassembly of Facially Amphiphilic Dendrimer Assemblies in Response to Physical, Chemical, and Biological Stimuli. *Acc. Chem. Res.* **2014**, *47*, 2200–2211.
47. Méndez, J.; Morales Cruz, M.; Delgado, Y.; Figueroa, C. M.; Orellano, E. A.; Morales, M.; Monteagudo, A.; Griebenow, K. Delivery of Chemically Glycosylated Cytochrome C Immobilized in Mesoporous Silica Nanoparticles Induces Apoptosis in HeLa Cancer Cells. *Mol. Pharm.* **2014**, *11*, 102–111.
48. Liu, C.; Wan, T.; Wang, H.; Zhang, S.; Ping, Y.; Cheng, Y. A Boronic Acid–Rich Dendrimer with Robust and Unprecedented Efficiency for Cytosolic Protein Delivery and CRISPR-Cas9 Gene Editing. *Sci. Adv.* **2019**, *5*, eaaw8922.
49. Ponta, H.; Sherman, L.; Herrlich, P. A. CD44: From Adhesion Molecules to Signalling Regulators. *Nat. Rev. Mol. Cell Biol.* **2003**, *4*, 33–45.
50. Faria, M.; Björnmalm, M.; Thurecht, K. J.; Kent, S. J.; Parton, R. G.; Kavallaris, M.; Johnston, A. P.; Gooding, J. J.; Corrie, S. R.; Boyd, B. J. Minimum Information Reporting in Bio–Nano Experimental Literature. *Nat. Nanotechnol.* **2018**, *13*, 777–785.
51. Ejima, H.; Richardson, J. J.; Liang, K.; Best, J. P.; van Koeverden, M. P.; Such, G. K.; Cui, J.; Caruso, F. One-Step Assembly of Coordination Complexes for Versatile Film and Particle Engineering. *Science* **2013**, *341*, 154–157.
52. Zhou, J.; Lin, Z.; Ju, Y.; Rahim, M. A.; Richardson, J. J.; Caruso, F. Polyphenol-Mediated Assembly for Particle Engineering. *Acc. Chem. Res.* **2020**, *53*, 1269–1278.

53. Lin, Z.; Zhou, J.; Cortez-Jugo, C.; Han, Y.; Ma, Y.; Pan, S.; Hanssen, E.; Richardson, J. J.; Caruso, F. Ordered Mesoporous Metal–Phenolic Network Particles. *J. Am. Chem. Soc.* **2020**, *142*, 335–341.
54. Yang, Y.; Bernardi, S.; Song, H.; Zhang, J.; Yu, M.; Reid, J. C.; Strounina, E.; Searles, D. J.; Yu, C. Anion Assisted Synthesis of Large Pore Hollow Dendritic Mesoporous Organosilica Nanoparticles: Understanding the Composition Gradient. *Chem. Mater.* **2016**, *28*, 704–707.
55. Shimizu, K.; Cha, J.; Stucky, G. D.; Morse, D. E. Silicatein α: Cathepsin L-Like Protein in Sponge Biosilica. *Proc. Natl. Acad. Sci. U.S.A.* **1998**, *95*, 6234–6238.

TOC Graphic

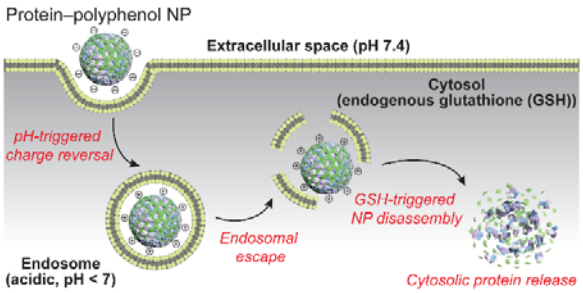
Protein–polyphenol NP
Extracellular space (pH 7.4)
Cytosol
(endogenous glutathione (GSH))
pH-triggered
charge reversal
GSH-triggered
NP disassembly
Endosomal
escape
Endosome
(acidic, pH < 7)
Cytosolic protein release